ELSEVIER

Energy and Buildings 33 (2001) 627–639

ENERGY AND BUILDINGS

www.elsevier.com/locate/enbuild

A two-layer turbulence model for simulating indoor airflow Part II. Applications

Weiran Xu, Qingyan Chen*

[a]*Department of Architecture, Massachusetts Institute of Technology, 77 Massachusetts Avenue, MA 02139, USA*

Received 2 August 2000; accepted 7 October 2000

Abstract

Energy efficient buildings should provide a thermally comfortable and healthy indoor environment. Most indoor airflows involve combined forced and natural convection (mixed convection). This paper used a two-layer model to predict such flows. This model used a one-equation model for near-wall region and the standard k–ε model for the outer-wall region. Its validation in six cases shows good agreements between the computed results and measured data. In addition, the computing cost required by the model has been reduced significantly. © 2001 Published by Elsevier Science B.V.

Keywords: Two-layer turbulence model; Indoor airflow; Computational fluid dynamics (CFD)

1. Introduction

Many airflows in building enclosures involve all three types of convection: forced, natural and mixed convection. Accurate simulation of these flows is essential for engineers to design, improve and optimize their ventilation systems and to save energy. This is because different airflow patterns can lead to different heat transfer coefficients and temperature distributions in a room. The air-conditioning load is related to the heat transfer coefficients and temperature distributions. With proper design of the ventilation systems, the air-conditioning load can be reduced. One typical example of this design is the displacement ventilation systems.

In order to calculate the indoor airflows, Xu and Chen (Part I) has recently developed a new two-layer turbulence model for predicting all three types of flows. The two-layer model solves a one-equation model in the near-wall region ($y^* < 80$) and the standard k–ε model [1] in the region away from walls. Therefore, in the near-wall region, k is solved by

$$\frac{\partial k}{\partial t} + U_i \frac{\partial k}{\partial x_i} = d_k + P_k + G_k - \varepsilon \tag{1}$$

the eddy viscosity is calculated by

$$v_t = \sqrt{\overline{vv}}\, l_\mu \tag{2}$$

ε by

$$\varepsilon = \frac{\sqrt{\overline{vv}}\, k}{l_\varepsilon} \tag{3}$$

l_μ, l_ε and $\overline{vv}/k$ by

$$l_\mu = \frac{(0.33 + 0.214 f_{l_\mu}) y}{1 + 5.025 \times 10^{-4} y_v^{*[1.53 + 0.12 f_{l_\mu}]}} \tag{4}$$

$$l_\varepsilon = \frac{(1.3 + 7.5 f_{l_\varepsilon}) y}{1 + (2.12 + 7.88 f_{l_\varepsilon})/y_v^* + (0.028 + 0.0235 f_{l_\varepsilon}) y_v^*} \tag{5}$$

$$\frac{\overline{vv}}{k} = 0.4 \left[1 - \exp\left(\frac{y^{*(2 - f_{vv/k})}}{4200(1 - 0.99 f_{vv/k})} \right) \right] \tag{6}$$

In the outer-wall region, where $y^* \geq 80$, the standard k–ε model [1] is used. The eddy viscosity is calculated by $v_t = C_\mu (k^2/\varepsilon)$ where $C_\mu = 0.09$. No length scale prescription is needed. This paper uses the new model for a number of engineering flows to demonstrate the performance of the model for forced, natural and mixed convection flows.

2. Applications of the new two-layer model to airflow simulations

This paper uses six cases to validate the new two-layer model. The validation has employed a CFD program, PHOENICS, as the solver. By default, PHOENICS uses

* Corresponding author.

0378-7788/01/$ – see front matter © 2001 Published by Elsevier Science B.V.
PII: S0378-7788(00)00130-4

Nomenclature

Ar_y	local Archimedes number, $g\beta\,\Delta T\,y_n/U^2$
Ar_b	bulk Archimedes number, $g\beta\,\Delta T\,L/U^2_{bulk}$
C_μ	constant used for calculating v_t
d_k	diffusion of turbulent kinetic energy
Fr	Froude number $U/\sqrt{g\beta\,\Delta T\,L}$
g	gravitational acceleration
g_i	component i of the gravitation vector
G_k	gravity production of turbulent kinetic energy, $-\beta g_i\overline{u_i t}$
h	convective heat transfer coefficient
k	turbulent kinetic energy, $\overline{u_i u_i}/2$
L	characteristic length
Nu_x	local Nusselt number, hx/λ_{air}
p	fluctuating pressure
P_k	shear production of the turbulent kinetic energy, $-\overline{u_i u_j}\partial U_i/\partial x_j$
Pr	Prandtl number
Pr_t	turbulent Prandtl number
P_t	total pressure
Ra	Rayleigh number, $\beta g\,\Delta T\,L^2/v\lambda$
Ra_x	local Rayleigh number, $\beta g\,\Delta T\,x^2/v\lambda$
Re	Reynolds number
t	fluctuating temperature or time
T	mean temperature
u, v	fluctuating velocity component in x, y direction, respectively
u_i	component i of fluctuating velocity
u_τ	friction velocity, $\sqrt{\tau_w/\rho}$
$\overline{u_i u_j}$	Reynolds stress
$\overline{u_i t}$	turbulent heat flux
U_i	component i of the mean velocity
U, V, W	mean velocity component in x, y and z direction, respectively
x, y, z	spatial coordinate
y_n	normal distance to the nearest wall
y^+, y^*, y^*_v	dimensionless wall distance, $y_n u_\tau/v, y_n\sqrt{k}/v, y_n\sqrt{vv}/v$

Greek symbols

β	thermal expansion coefficient $-(1/\rho)(\partial\rho/\partial T)$
δ_{ij}	Kronecker delta
ε	turbulent energy dissipation
λ	thermal conductivity
v	molecular viscosity
v_t	turbulent viscosity
ρ	fluid density
σ_k, σ_ε	Prandtl number of k and ε
τ_w	wall shear stress

Superscripts

–	time-averaged quantities
∼	instantaneous quantities
+	non-dimensionalized by wall-friction quantities

Subscripts

i, j	spatial coordinate indices
ref	reference conditions
t	turbulent quantities

the upwind difference scheme to discretize the convection term in the governing equation. The staggered grids and SIMPLEST [2] method were used to decouple the pressure and velocity fields. We adopted the power-law spacing method [2] to distribute grids. The iteration uses the linear relaxation for the pressure and the false-time-step method for all other variables. The convergence criterion was set such that the respective sums of the absolute residuals of sources of U, V, W, P, T, k and ε must be less than 10^{-3} of their inflow flux, where P actually refers to the continuity equation.

We have applied the new model in forced, natural and mixed convection cases. The following section describes the computation procedure and the results of these cases.

2.1. Forced convection

Forced convection flows are often encountered in rooms when buoyancy effects in air are very small. This section tests the performance of the new model in two forced convection cases: a simple channel flow and a forced convection flow in a room.

2.1.1. Airflow between two parallel infinitely long plates ($Gr = 0.0$)

2.1.1.1. Flow conditions. The geometry of this case has been shown in Fig. 1. This is a typical Couette–Poiseuille flow and has many practical applications, such as the flows in a duct. Several DNS studies, including those by Kim et al. [3] and Kuroda et al. [4], have been conducted for this type of flows. In order to compare the results predicted by the new model with the DNS data, the Reynolds number used in the current computation is 4358, the same as that used in the DNS study [5].

2.1.1.2. Boundary conditions and computation details. Since the plates are infinitely long, the fully developed conditions are applicable. The pressure gradient in the

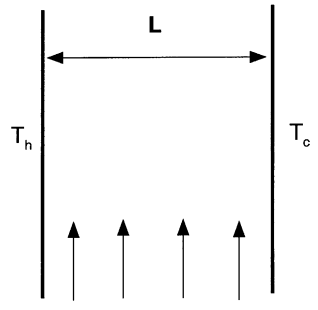

Fig. 1. The configuration used in the DNS study [5].

fully developed channel flow is a non-zero constant. Without knowing the pressure gradient, we have used the parabolic conditions in our calculation. The parabolic conditions imply that the flow will not be influenced by downstream conditions. Next, the length to be calculated in the x direction is set to $100L$ to ensure no entrance effects on the results.

The application of the parabolic conditions allows the specification of uniform velocity at the channel entrance. The boundary conditions at the plates are the no-slip for velocity U and fixed temperature for temperature T, respectively. The turbulent kinetic energy is zero at the plates. The turbulence dissipation rate ε is determined from Eq. (3). Table 1 summarizes the boundary conditions and provides the relaxation method and factors used in the computation.

2.1.1.3. Results and discussions. The results with different grids are shown in Fig. 2. All the physical quantities are non-dimensionalized by the wall-friction velocity, viscosity or the temperature difference. We have used 20, 30 and 36 grids non-uniformly which distribute 5, 7 and 11 points, respectively, under $y^* < 80$ on each side. Fig. 2a and b show that the computed mean velocity and temperature profiles agree with the DNS data excellently. Other quantities compared are k, ε, v_t, and the root-mean-square of the normal-to-wall Reynolds stress component, v_{rms}. The results agree with the DNS data very well.

The results indicate that five grids in the inner-wall region ($y^* < 80$) are sufficient. A further increase of grids does not significantly improve the accuracy. This requirement is much less than that of a LRN model, which usually needs about 20 grids in a similar range. The computational saving due to the grid deduction is very significant, especially in a 3D application.

2.1.2. Airflow in a ventilated room (L:H = 3:1)

2.1.2.1. Flow conditions. This section will examine the performance of the new two-layer model for the flow in an isothermally ventilated room. Fig. 3a shows the configuration of the room. The length to height ratio (L:H) is 3:1. The Reynolds number based on the inlet height is 5000. Restivo [6] had conducted an experiment in this configuration and measured the mean velocity and velocity fluctuation in the room by a LDV system. The experimental data have extensively used by many researchers to validate the numerical predictions for this case [7–9].

2.1.2.2. Boundary conditions and computation details. The boundary conditions that need to be supplied to the calculations are those at the walls, inlet and outlet. Our computation has specified no-slip boundary conditions for velocity at all walls, uniform velocity distribution for the inlet and zero reference pressure at the outlet. The turbulent kinetic energy and dissipation at inlet and outlet are specified empirically. The grid number used was 40×30. Table 2 provides details of the boundary conditions and computational parameters for the present calculation.

2.1.2.3. Results and discussions. Fig. 3b displays the calculated flow pattern of this case. The flow pattern agrees with that obtained by other researchers, e.g. Chen [8]. The normalized mean velocity and fluctuation profiles at two vertical ($x/H = 1.0,\ 2.0$) and two horizontal ($y/H = 0.028,\ 0.972$) locations have been presented in Figs. 4 and 5, respectively. The predicted mean velocity profile at $x/H = 1.0$ and 2.0 agree with the experimental data very well, as shown in Fig. 4a and b. Fig. 4c and d present the velocity profiles in the region close to the ceiling and the floor, respectively. The trend and magnitude of the predicted velocities agree with the measured data except at the room's upper-right and lower-left corners, where two small eddies occur. The small eddies are called secondary flows that usually cannot be predicted by a one- or two-equation model. To capture the small eddies, an anisotropic turbulence model such as a RSM has to be used [8]. Applying a RSM in the computation is quite complex and expensive and has little practical interests for a designer.

The agreement of the predicted root-mean-square fluctuations in x direction is not as good as that of the mean velocity, especially in the corners, as shown in Fig. 5. One possible reason is that the model calculates the turbulent kinetic energy $k = (\overline{u}^2 + \overline{v}^2 + \overline{w}^2)/2$ instead of the individual component. The eddy-viscosity assumption $\overline{u}^2 = -2(\partial U/\partial x) + (2/3)k$ has to be used to obtain the u_{rms} distribution. This assumption, however, is not accurate especially with anisotropic turbulence. On the other hand, the performance of the

Table 1
Boundary conditions and computation details

	P	U	T	k	ε
B.C.[a] at channel entrance	–[b]	U_{bulk}	T_{bulk}	0	0
B.C.[a] at channel end	0	$\frac{\partial U}{\partial x} = 0$	$\frac{\partial T}{\partial x} = 0$	$\frac{\partial k}{\partial x} = 0$	$\frac{\partial \varepsilon}{\partial x} = 0$
B.C.[a] at walls (plates)	–[b]	0	T_w	0	Eq. (3)
Relaxation method	Linear relaxation	False-time-step	False-time-step	False-time-step	False-time-step
Relaxation factor	0.8	100	1	0.1	0.1

[a] Boundary conditions.
[b] No need to specify.

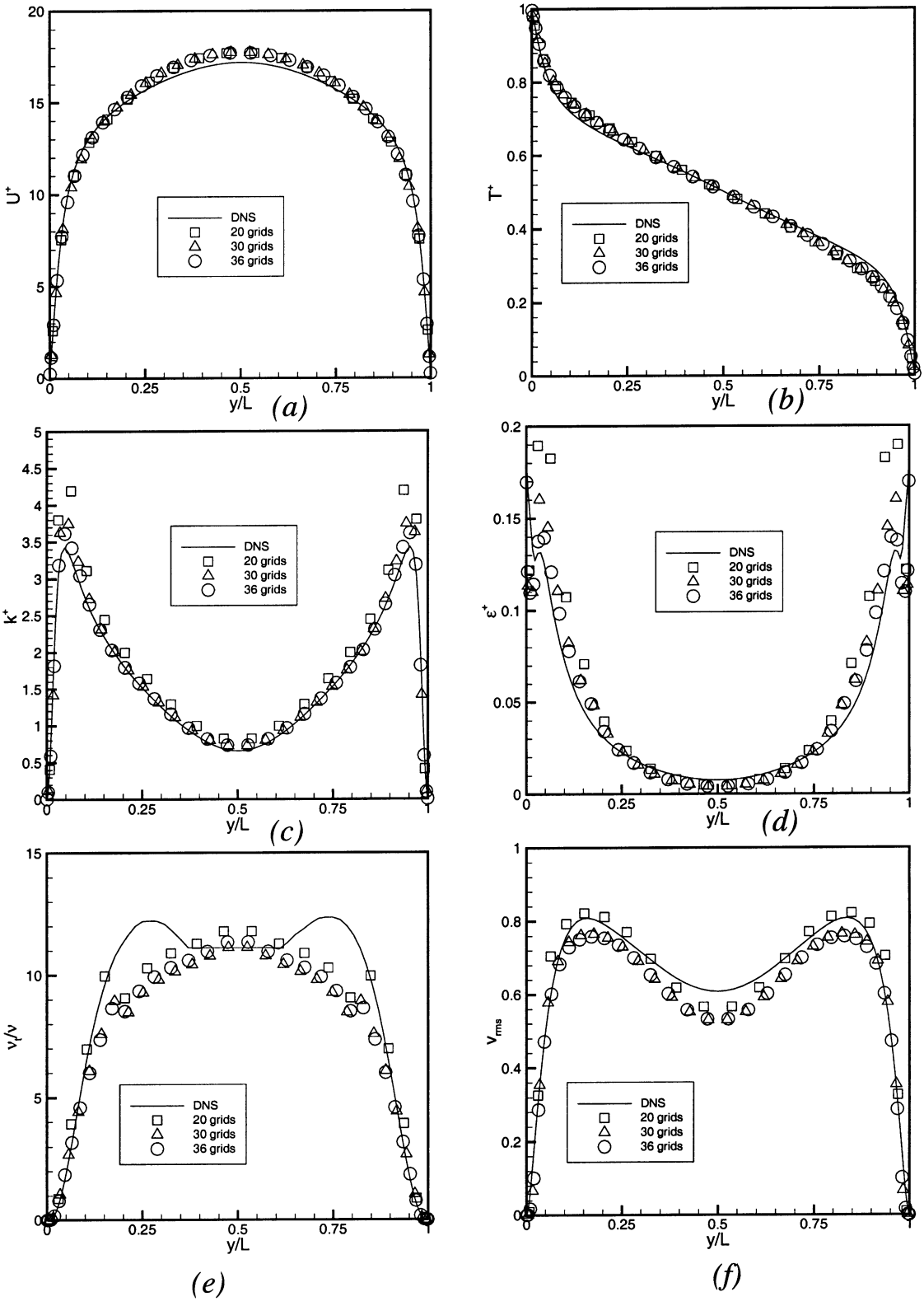

Fig. 2. Comparison of the prediction of Case 1 with the DNS data [5]: (a) mean velocity; (b) mean temperature; (c) k; (d) ε; (e) v_t; (f) v_{rms}.

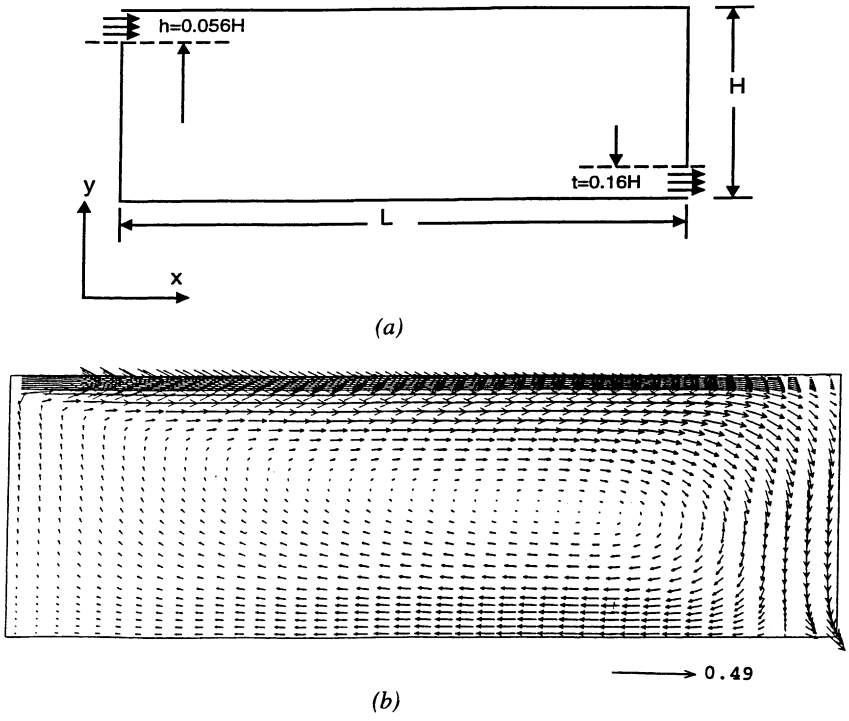

Fig. 3. Forced convection case. (a) Sketch of the room with forced convection; (b) predicted flow pattern.

new model is at least comparable to other forced-convection models in predicting the fluctuations, as shown by Chen [7].

The results from the two forced convection cases suggest that the new model performs well in isothermal flows.

2.2. Natural convection

Natural convection is an important phenomenon in room airflow and must be predicted correctly. This section verifies the applicability of the new two-layer model in predicting natural convection flows.

2.2.1. Airflow along infinitely long plates ($Ra = 5.4 \times 10^5$)

This section applies the new model to the case of natural convection between a pair of infinitely long, parallel and differentially heated plates. The Rayleigh number is 5.4×10^5. Versteegh and Nieuwstadt [10] have performed DNS study for this geometry and Rayleigh number.

The boundary conditions are set as: no-slip boundary conditions for the velocity; fixed temperature for the walls. Table 3 lists the relaxation factors used for this case. Twenty grids were used in the present computation. Fig. 6 illustrates the calculated mean velocity, temperature, turbulent kinetic energy and turbulent energy dissipation. The solid lines in the figure represent the DNS results from Versteegh and Nieuwstadt [10]. The mean velocity and temperature agree with the DNS data very well but the turbulent energy and dissipation are under-predicted. The reason is that the gravity production becomes zero under the eddy-viscosity assumption. The results obtained in this paper confirm that the new model has been successfully transformed to the natural convection model [11] as desired.

Table 2
The details of the boundary conditions and computational parameters for predicting the forced convection flow in a room

	P	U	T	k	ε
B.C.[a] at inlet	–[b]	U_{in}	0	$2.4 \times 10^{-3} U_{in}^2$	$\frac{k_{in}^{3/2}}{0.1h}$
B.C.[a] at outlet	0	$\frac{\partial U}{\partial x} = 0$	$\frac{\partial V}{\partial x} = 0$	$\frac{\partial k}{\partial x} = 0$	$\frac{\partial \varepsilon}{\partial x} = 0$
B.C.[a] at walls	–[b]	0	0	0	Eq. (3)
Relaxation method	Linear relaxation	False-time-step	False-time-step	False-time-step	False-time-step
Relaxation factor	0.8	100	1	0.1	0.1

[a] Boundary conditions.
[b] No need to specify.

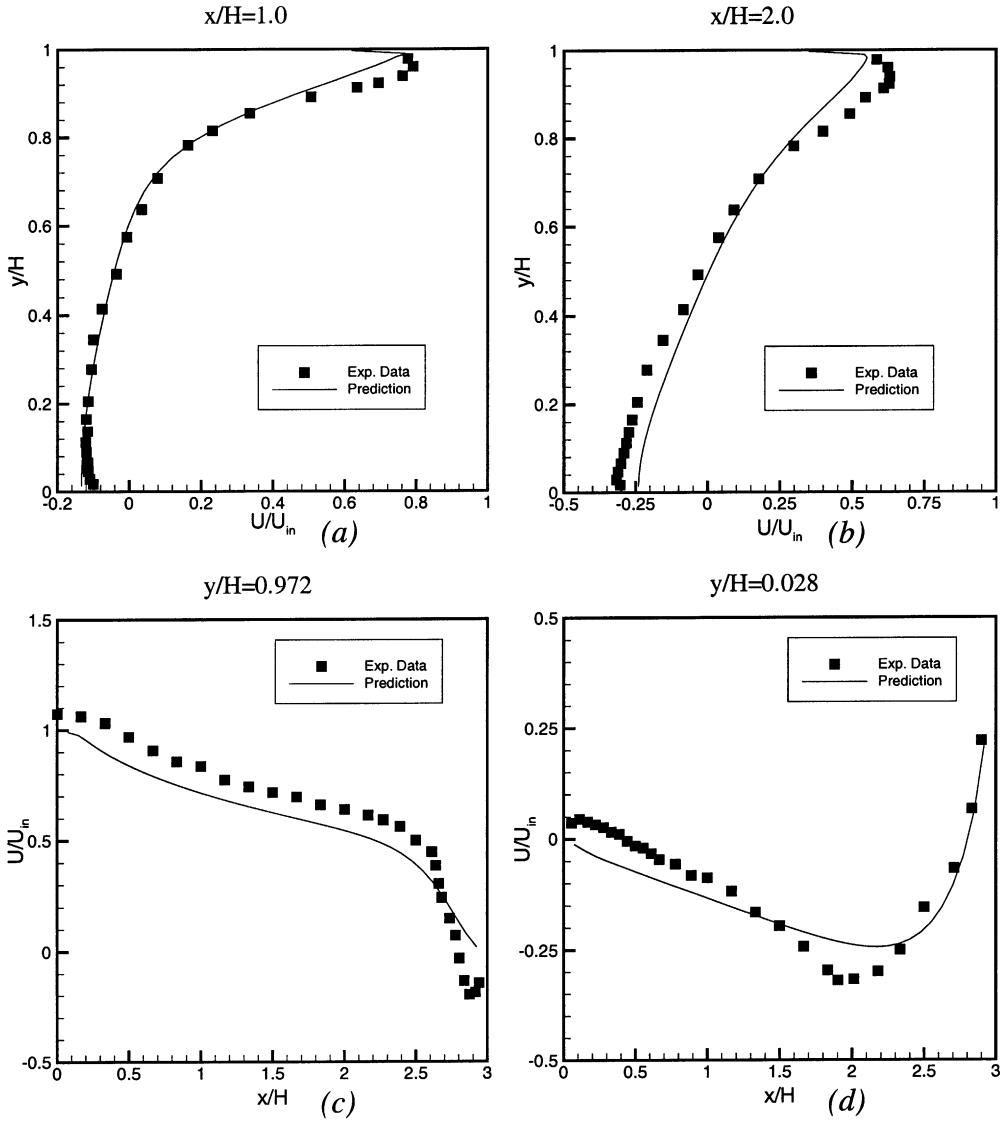

Fig. 4. Comparison of the predicted mean velocity with the experimental data [6]. (a) $x/H = 1.0$; (b) $x/H = 2.0$; (c) $y/H = 0.972$; (d) $y/H = 0.028$.

2.2.2. Airflow in a room with differentially heated walls (L:H= 1:5)

In this section, natural convection in a tall cavity of 0.5 m width and 2.5 m height is investigated numerically with the two-layer model just developed. Cheesewright et al. [12] conducted experimental studies on natural convection in this cavity. Their experiments maintained isothermal conditions (65.8 and 20°C) on the two vertical walls and insulated the two horizontal walls, although, they were not ideally insulated. The Rayleigh number based on cavity height was 5×10^{10}.

Fig. 7a shows the geometry and boundary conditions adopted in the numerical simulation for this case. The relaxation factors are listed in Table 4. The numerical simulation uses the isothermal boundary condition for the two vertical walls and adiabatic conditions for the horizontal walls. No-slip and zero-k conditions were applied at all walls. No boundary condition for ε was necessary since ε is determined by Eq. (3) in the boundary layer.

The predicted mean velocities are in good agreement with the experimental data [12] as shown in Fig. 7b. The predicted temperatures are higher than the measured ones. This is because the experimental cavity had imperfect insulation on the top and bottom wall [12] while the computation used adiabatic conditions for those walls. Fig. 7d shows that though the peaks of the velocity fluctuation were under-predicted, the trend agrees well with the measurements. Fig. 7e shows the computed and measured local Nusselt number with respect to the local Rayleigh number. The agreement between the prediction and the experimental data is very good.

The two validation cases have proved that the new two-layer model performs well in natural convection cases. The next section will study the capability of the new model in predicting mixed convection flows.

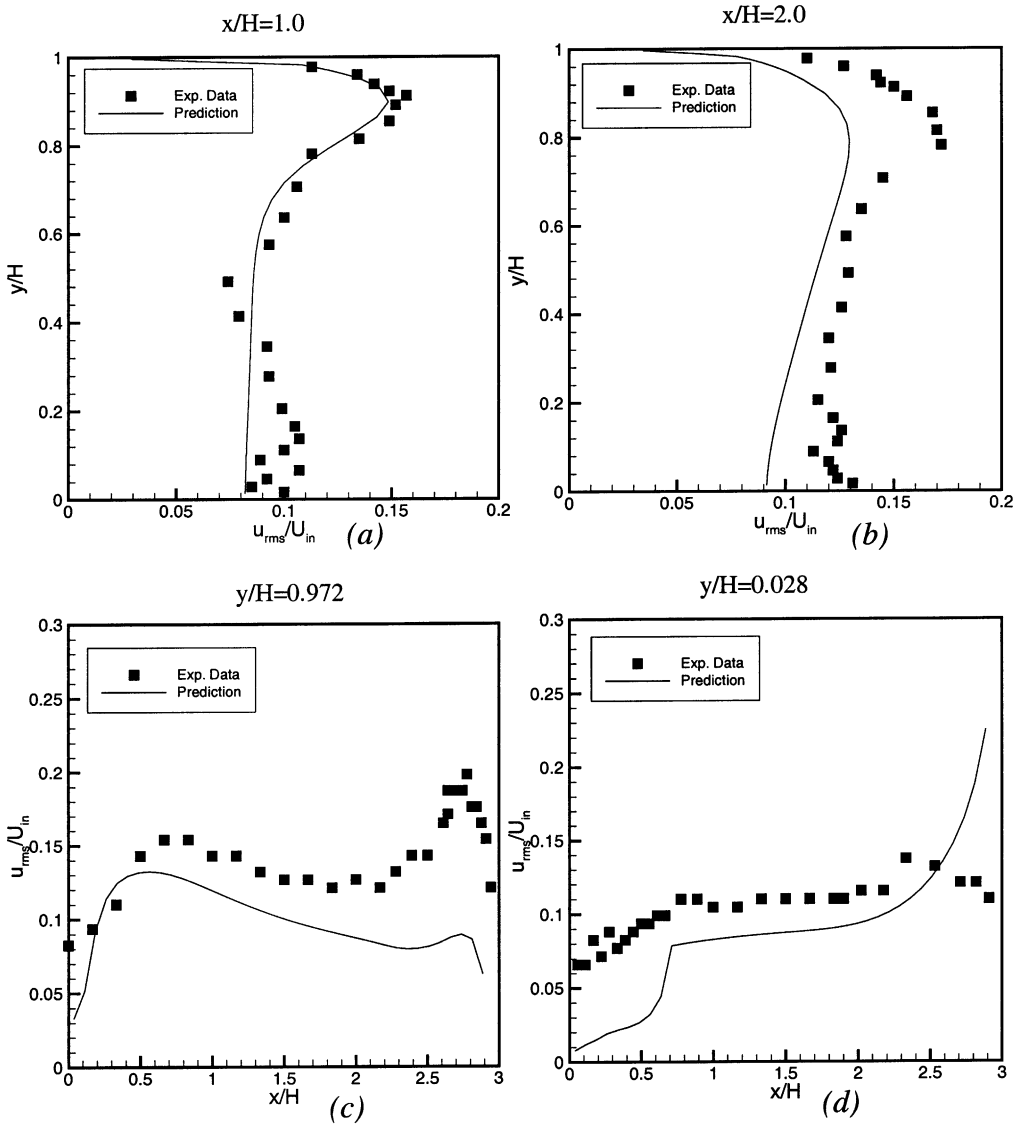

Fig. 5. Comparison of the predicted velocity fluctuation u_{rms} with the experimental data [6]. (a) $x/H = 1.0$; (b) $x/H = 2.0$; (c) $y/H = 0.972$; (d) $y/H = 0.028$.

2.3. Mixed convection

Mixed convection is the most common flow encountered indoors, such as in summer when air conditioners are turned on. This section applies the new two-layer model to two validating cases, including a mixed convection flow between two plates, in rooms with weak and strong buoyancy effects, and in an office with several heat and contaminant sources.

2.3.1. Airflow in a ventilated room with a heated wall (L:H = 4.7:1)

2.3.1.1. Flow conditions. Mixed convection in a ventilated room with a heated wall is calculated in this section. The configuration is similar to that in Fig. 3a but with a different length-to-height ratio (4.7:1) and inlet size ($0.025H$). The outlet location and size is $0.16H$, the same as the one shown in Fig. 3a. The wall right above the outlet was heated so that

Table 3
Relaxation method and factors used in Section 2.2.1

	P	U	T	k	ε
Relaxation method	Linear relaxation	False-time-step	False-time-step	False-time-step	False-time-step
Factor	0.8	100	1	0.1	1

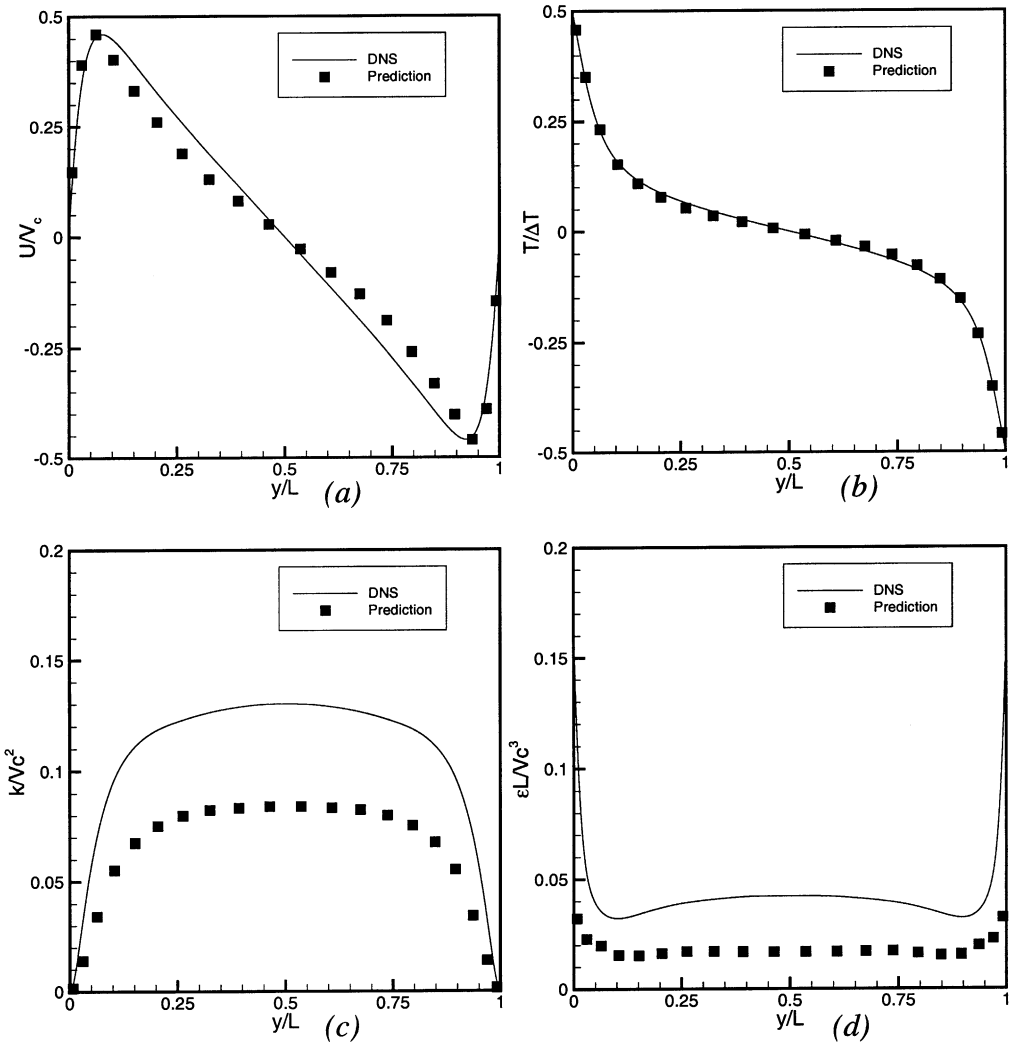

Fig. 6. Comparison of the predicted results with the DNS data [10] for natural convection between two infinitely long plates. (a) Mean velocity; (b) mean temperature; (c) k; (d) ε.

a buoyant wall jet occurs, travels along the ceiling and meets the wall-jet from the inlet. Then the collapsed stream goes down to the floor, splits into two opposite directions and forms two large eddies in the room (see Fig. 8a). The length between the inlet and the location where two jets meet is called the penetration length, x_e. The penetration length is important for an engineer to design a ventilation system to prevent the draft or over-throw conditions. Schwenke [13] conducted a series of experiments and measured the penetration length under various Archimedes numbers. The Archimedes number was defined as:

$$Ar = \frac{g\beta(T_{out} - T_{in})h}{U_{in}^2} \tag{7}$$

where h is the inlet size and U_{in} is the inlet velocity. This definition is convenient but not a good measure of the relative importance of buoyancy and inertia in rooms, since the velocities in rooms are usually low and the length scale is large. We have selected Schwenke's data to validate the new model.

2.3.1.2. Boundary conditions and computation details. The boundary conditions are similar to those used in Section 2.1.2. In addition, the boundary conditions for the mean temperature have to be provided. Table 5 lists the boundary conditions and the relaxation details used in the calculation. The current study used 60×49 grids.

2.3.1.3. Results and discussions. The calculated penetration lengths under various Ar are compared with the data [13] and shown in Fig. 8. The agreement between the experimental data and the calculated results is fairly good. Chen [7] applied the several LRN KEMs to this case with 110×70 grids and found that the performance of those models were not satisfactory. The new model was found superior to the LRN models but, at the same time, the grid

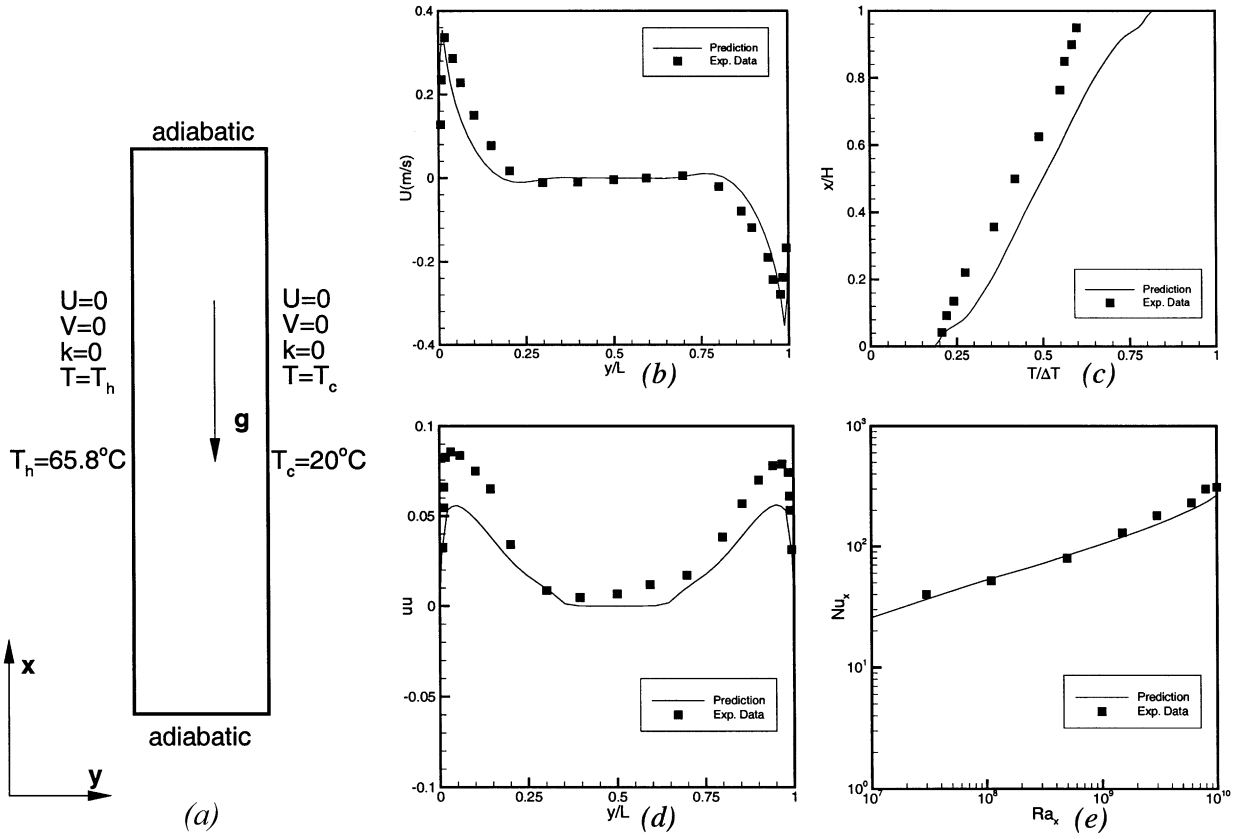

Fig. 7. Comparison of the predicted results with the experimental data [12] for natural convection in a 5:1 cavity. (a) Geometry and boundary conditions; (b) mean velocity at the mid-height; (c) mean temperature at the mid-width; (d) velocity fluctuation; (e) local Nusselt number.

number needed in the case was significantly less than those models. The new model appears to be more accurate and cost-effective than the existing models.

So far, the cases we have studied involve mixed convection with heated vertical surfaces. The next sections apply the new model to mixed convection with heated horizontal surfaces.

2.3.2. Airflow in a ventilated room with heated floor (L:H = 1:1)

The last section shows that the new model performs well under small buoyancy effects. This section uses the experimental data from Blay et al. [14] to test the model in predicting a flow under stronger buoyancy effects.

2.3.2.1. Flow conditions. Blay's experiment [14] was conducted in a 2D cavity as shown in Fig. 9. Although the configuration is a laboratory model rather than an actual room, the flow is mixed convection and represents flow features found in actual rooms.

The experiment maintained a temperature, $T_w = 15^\circ C$, at the two vertical walls and the top wall while the floor was heated to a higher temperature, $T_{fl} = 35.5^\circ C$. An air jet with a temperature $T_{in} = T_w$ was discharged horizontally into the cavity at a velocity that varied from 0.25 to 0.57 m/s. The experiment found that the overall flow circulation could vary from a clockwise to an anti-clockwise direction depending on the jet Froude number $Fr = U_{in}/g\beta(T_{fl} - T_{in}) = 1/\sqrt{Ar}$.

The mean velocity, temperature and turbulent kinetic energy at $x/L = 0.5$ and $y/L = 0.5$ were measured with an inlet velocity 0.57 m/s. According to the experimental conditions, the present study sets the following boundary conditions for the computation: no-slip condition for the velocity and constant temperature condition for the temperature at walls; uniform velocity $U_{in} = 0.57$ m/s and temperature $T_{in} = 15^\circ C$ at inlet; zero pressure at outlet;

Table 4
Relaxation method and factors used in Cheesewright's case [12]

	P	U	V	T	k	ε
Relaxation method	Linear relaxation	False-time-step	False-time-step	False-time-step	False-time-step	False-time-step
Factor	0.8	0.1	0.1	0.1	0.1	0.1

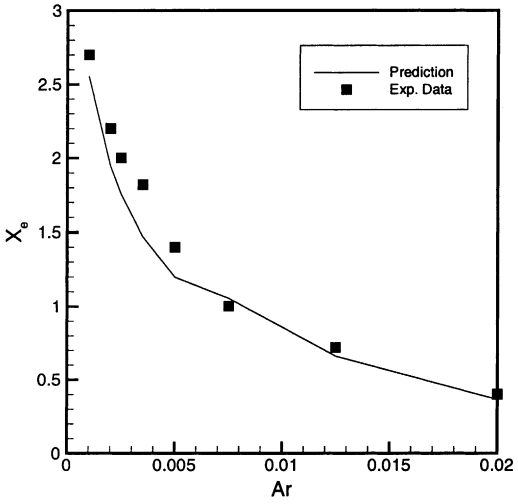

Fig. 8. Comparison of the predicted penetration length with experimental data [13].

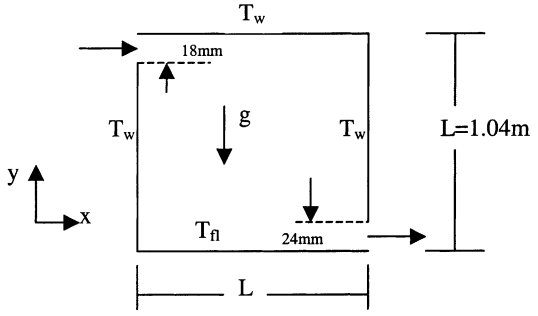

Fig. 9. The 2D configuration used in Blay's experiment [14] and the current calculation.

and zero k at all walls. At the inlet k is set to 1.25×10^{-3} (m^2/s^2), which corresponds to a measured turbulence intensity of 6%. The dissipation at the inlet, ε_{in}, is set to zero. Three sets of grid numbers, 35×32, 40×40, 50×50 were used for grid-dependent study. The relaxation methods and factors are listed in Table 6.

2.3.2.2. Results and discussions. The calculated and measured flow patterns are compared in Fig. 10, where Fig. 10a shows the measured flow pattern. Fig. 10b shows that the computation captured all major characters of the flow pattern observed in the experiment, such as the main eddy in the center of the cavity and the small eddy close to the inlet jet. In order to verify the new two-layer model further, we have calculated another case with the inlet velocity $U_{in} = 0.25$ m/s, which corresponds to a low Froude number 2.32. The experiment revealed that the flow pattern under such a *Fr* number was an anti-clockwise type. Fig. 10d shows that the computed flow pattern agrees with the experimental findings (Fig. 10c).

The grid-dependent study was conducted and the results are shown in Fig. 11, which compares the measured mean velocity at $x/L = 0.5$ [14] with the computational results obtained with 35×32, 40×40 and 50×50 grids. The comparison indicates that the calculation with 35×32 grids has already produced accurate results. Increasing the resolution does not yield a significant difference and improvement. Thus, the following comparisons employ only the results obtained by 35×32 grids.

Fig. 12 compare the mean velocity, temperature, and turbulent kinetic energy between the computed results

Table 5
Boundary conditions and computation details for Schwenke's case

	P	U	V	T	k	ε
B.C.[a] at inlet	–[b]	U_{in}	0	T_{in}	$2.4 \times 10^{-3} U_{in}^2$	$\frac{k_{in}^{3/2}}{0.1h}$
B.C.[a] at outlet	0	$\frac{\partial U}{\partial x} = 0$	$\frac{\partial V}{\partial x} = 0$	$\frac{\partial T}{\partial x} = 0$	$\frac{\partial k}{\partial x} = 0$	$\frac{\partial \varepsilon}{\partial x} = 0$
B.C.[a] at walls	–[b]	0	0	Constant heat flux on east wall otherwise $\frac{\partial T}{\partial x} = 0$	0	Eq. (3)
Relaxation method	Linear relaxation	False-time-step	False-time-step	False-time-step	False-time-step	False-time-step
Relaxation factor	0.8	1.1	1.1	2.8	0.3	0.3

[a] Boundary conditions.
[b] No need to specify.

Table 6
Relaxation method and factors used in Blay's case

	P	U	V	T	k	ε
Relaxation method	Linear relaxation	False-time-step	False-time-step	False-time-step	False-time-step	False-time-step
Factor	0.8	1.44	1.44	8.64	0.288	0.288

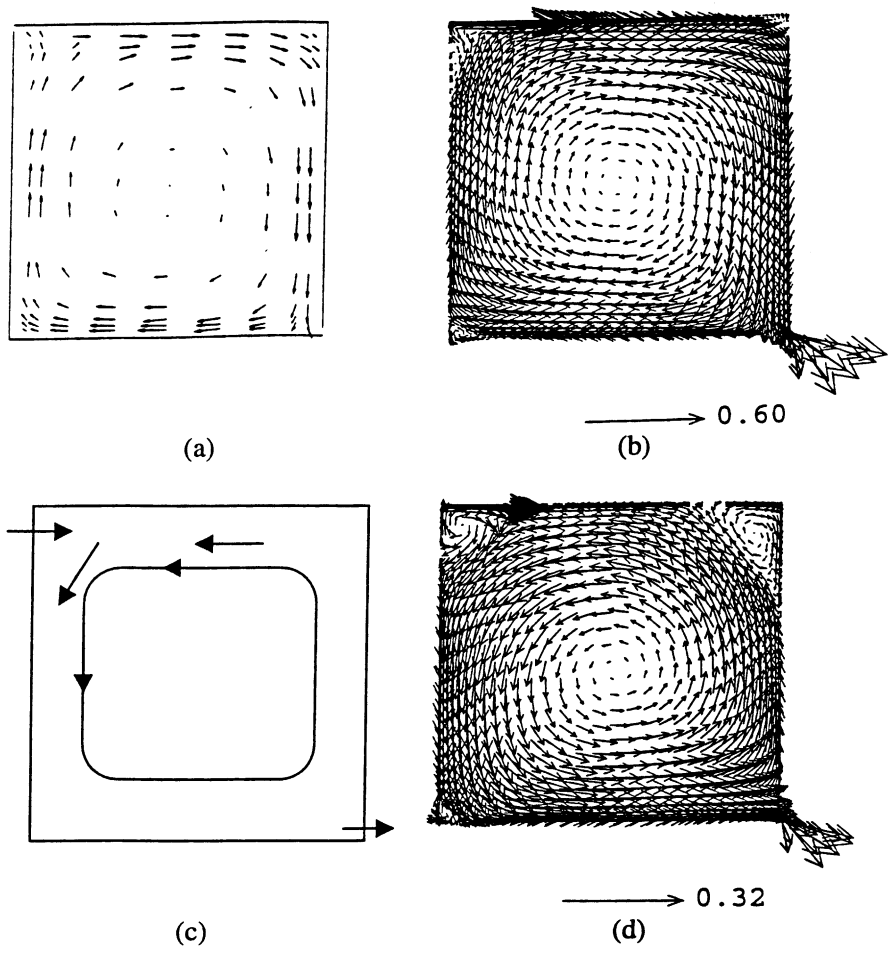

Fig. 10. Mixed convection in a 1:1 cavity. (a) Observed flow pattern at $Fr = 5.31$; (b) predicted flow pattern at $Fr = 5.31$; (c) observed flow pattern at $Fr < Fr_c$ (2–3.4); (d) predicted flow pattern at $Fr = 2.32$.

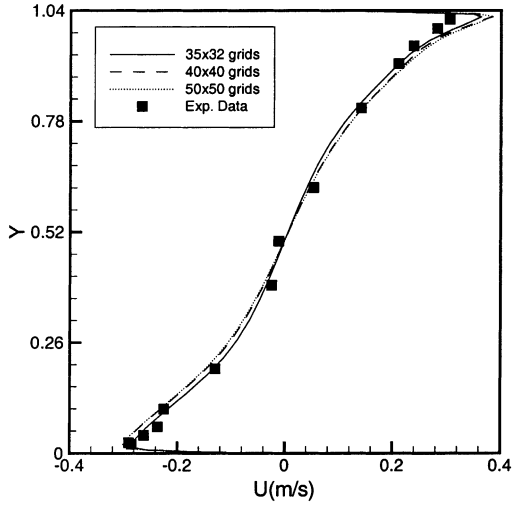

Fig. 11. Grid-dependent study: mean velocity comparison at $x/H = 0.5$. Experimental data from [14].

and the experimental data [14] at $x/H = 0.5$ and $y/H = 0.5$. Fig. 12a and b show that though the peaks of the velocity were over-predicted, the overall agreement of the velocity is very good. The temperature prediction also agrees well with the data. The largest difference between the numerical results and the data is less than 1 K, as shown in Fig. 12c and d. Fig. 12e and f illustrate that the predicted turbulent energy reasonably agrees with the measured data, although the agreement is not as good as the mean quantities.

In addition to the measurements, Blay et al. [14] has performed a numerical simulation for the above case with Jones–Launder [15] and Lam–Bremhorst LRN KEMs [16]. They found that the Jones–Launder's model failed while Lam–Bremhorst model reproduced the experimental data quite well. Their grid-dependent study found that at least 52×52 grids are needed to produce acceptable results. The current study has reduced the grid requirement by 58% while retaining the accuracy of the prediction.

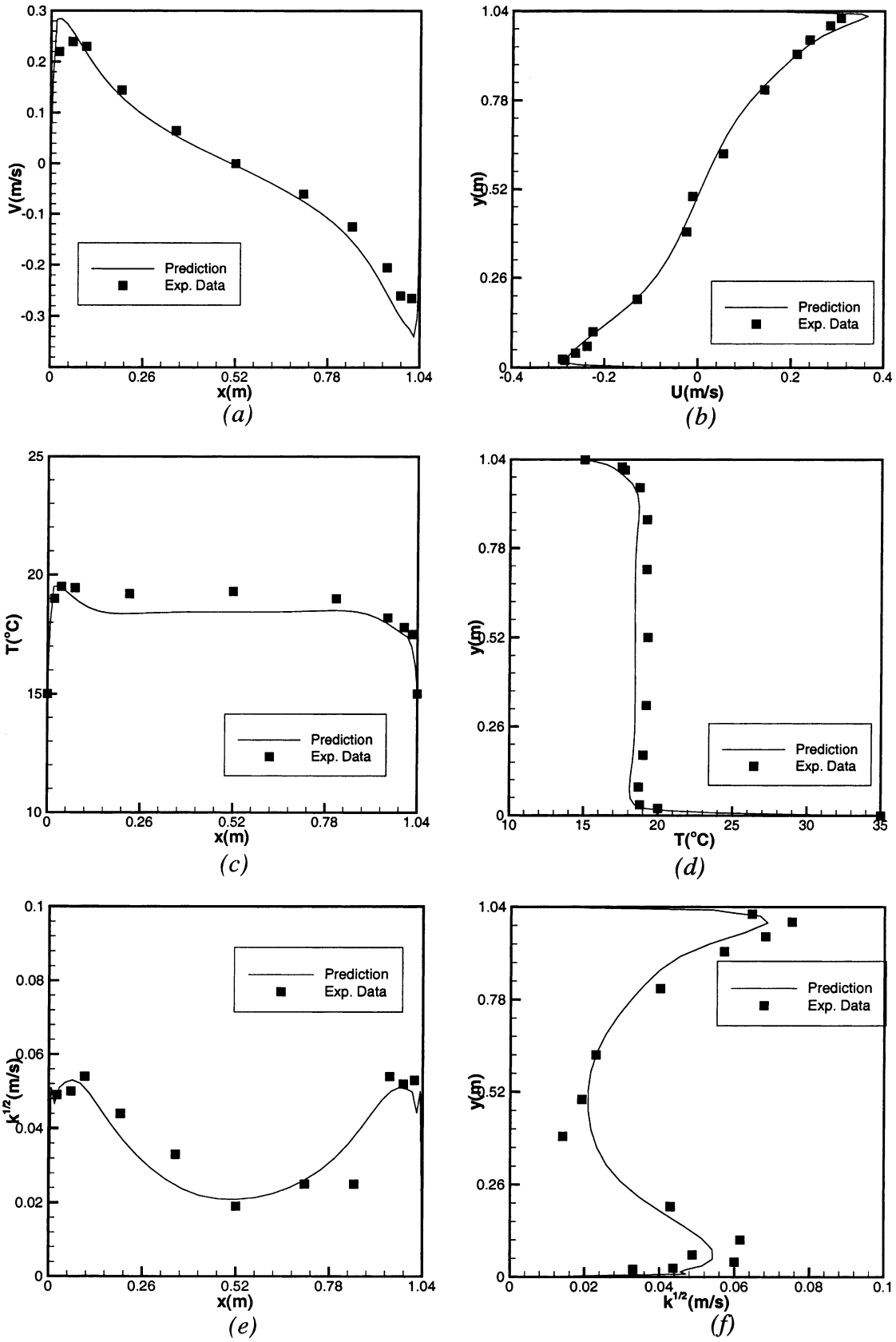

Fig. 12. Comparison of the predicted results with the experimental data [14]. (a) Mean velocity at $y/L = 0.5$; (b) mean velocity at $x/L = 0.5$; (c) mean temperature at $y/L = 0.5$; (d) mean temperature at $x/L = 0.5$; (e) $k^{1/2}$ at $y/L = 0.5$; (f) $k^{1/2}$ at $x/L = 0.5$.

3. Conclusions

By studying flows in channels, cavities and real-size rooms, this paper has validated a two-layer turbulence model for predicting forced, natural, and mixed convection airflow. This model appears to be accurate and cost-for applications in indoor airflows. The model also permits the use of a single model to analyze flows with various buoyancy conditions.

Acknowledgements

This study is supported by the National Science Foundations through Grant CMS-9623864.

References

[1] B.E. Launder, D.B. Spalding, The numerical computation of turbulent flows, Computer Methods in Applied Mechanics and Energy 3 (1974) 269–289.
[2] D.B. Spalding, The PHOENICS Encyclopedia, 1994, CHAM, Ltd., London, UK.
[3] J. Kim, P. Moin, R. Moser, Turbulence statistics in fully developed channel flow at low Reynolds number, Journal of Fluid Mechanics 177 (1987) 133–166.
[4] A. Kuroda, N. Kasagi, M. Hirata, Direct numerical simulation of turbulent plate Coutte–Poiseulle flow: effects of mean shear rate on the near-wall turbulence structures, in: Turbulent Shear Flows, Vol. 9, Springer, Berlin, 1994, pp. 241–258.
[5] N. Kasagi, M. Nishimura, Direct numerical simulation of combined forced and natural convection in a vertical plane channel, International Journal of Heat and Fluid Flow 18 (1997) 88–99.
[6] A. Restivo, Turbulent flow in ventilated rooms, Ph.D. Thesis, University of London, UK, 1979.
[7] Q. Chen, Comparison of different k–ε models for indoor air flow computations, Numerical Heat Transfer: Part B 28 (1995) 353–369.
[8] Q. Chen, Prediction of room air motion by Reynolds-stress models, Building and Environment 31 (1996) 233–244.
[9] P. Emvin, The full multigrid method applied to turbulent flow in ventilated enclosures using structured and unstructured grids, Ph.D. Thesis, Charlmers University of Technology, Sweden, 1997.
[10] T.A.M. Versteegh, F.T.M. Nieuwstadt, Scaling of free convection between two differentially heated infinite vertical plates, in: Turbulent Shear Flow, Vol. 11, 1996.
[11] W. Xu, Q. Chen, F.T.M. Nieuwstadt, A new turbulence model for near-wall natural convection, International Journal of Heat Mass Transfer 41 (1998) 3161–3176.
[12] R. Cheesewright, K.J. King, S. Ziai, Experimental data for validation of computer codes for prediction of two-dimensional buoyant cavity flows, in: J.A.C. Humphrey, C.T. Adedisian, B.W. le Tourneau (Eds.), Significant Questions in Buoyancy Affected Enclosure or Cavity Flows, 1986, ASME, pp. 75–81.
[13] H. Schwenke, Ueber das Verhalten elener horizontaler Zuluftstrahlen im begrenzten Raum, Luft- und Kaltetechnik 5 (1975) 241–246.
[14] D. Blay, S. Mergui, C. Niculae, Confined turbulent mixed convection in the presence of a horizontal buoyant wall jet, Fundamentals of Mixed Convection HTD 213 (1992) 65–72.
[15] W.P. Johns, B.E. Launder, Prediction of laminarization with a two-equation model of turbulence, International Journal of Heat Mass Transfer 34 (1972) 301–314.
[16] C.K.G. Lam, K.A. Bremhorst, Modified form of k–ε model for predicting wall turbulence, Journal of Fluids Engineering, ASME Transactions 103 (1981) 456–460.